

## Measurement of Water Vapour in Axisymmetric Jet Development Using TDLAS

A. Al-Manea<sup>1,2</sup>, D. Buttsworth<sup>1</sup>, J. Leis<sup>1</sup>, R. Choudhury<sup>1</sup> and K. Saleh<sup>1</sup>

<sup>1</sup> School of Mechanical and Electrical Engineering  
 University of Southern Queensland, Toowoomba, Queensland, 4350, Australia

<sup>2</sup>Al-Samawah Technical Institute  
 Al-Furat Al-Awsat Technical University, Al-Samawah, 66001, Iraq

### Abstract

Turbulent mixing of multi-phase compressible jets formed within steam ejectors requires further investigation so that reliable models can be developed to aid in the ejector design process. As a step towards the non-intrusive measurement of the flow conditions in such a jet, tunable diode laser absorption spectroscopy (TDLAS) is used to investigate the development of an axisymmetric subsonic jet of air containing a high concentration of water vapour (with a relative humidity around 70%), and a co-flowing stream of dry nitrogen. The radius of the jet nozzle was 14 mm and the measurements were made at distances of 5, 10, and 15 mm downstream of the nozzle exit. At each downstream distance, TDLAS measurements of water vapour features at around 1392 nm were made using a discrete mode laser. At each measurement location, the absorbance was recorded and the water vapour concentration was determined by using an Abel inversion and by fitting spectral results from the HITRAN 2012 database to the measured spectra using custom MATLAB scripts. Simulation of the experimental jet conditions was used to assess the accuracy of analysis method, and results indicate an accuracy of better than  $\pm 5\%$  in the water vapour concentration can be achieved using the method proposed in this paper.

### Introduction

The development of jet mixing plays a critical role in steam ejectors which are used in a wide variety of industrial applications to induce pumping and compression effects. For typical steam ejector operating conditions, the primary flow of steam experiences a non-equilibrium condensation process within the jet nozzle prior to the development of compressible, turbulent mixing with the surrounding flow. For the development of improved ejector devices, reliable simulation tools are required, but the modelling of the compressible turbulent mixing of wet steam flows is challenging because of the number and complexity of interacting physical processes: non-equilibrium multi-phase turbulent compressible flow with strong pressure gradients, including shock waves [3].

Over the past decades, significant work has been performed in the area of TDLAS techniques [11]. Measurements of the temperature and water mole fraction using this technique have been extensively studied and implemented for flame measurement [4, 5]. This study seeks to apply TDLAS (tunable diode laser absorption spectroscopy) to the measurement of steam ejector mixing flows, in order to obtain experimental data that can be used for model development and validation. However, because of the significant complexities associated with such ejector flow conditions, we have chosen to tackle a simplified steam jet mixing problem to assess and optimize the technique, and to develop methods to reconstruct the water-vapour concentration distribution at different locations downstream from the nozzle.

### TDLAS theoretical background

The TDLAS technique is well established [11]. Transmission of light at a particular wavelength, through a particular medium, can be described by the Beer-Lambert relation:

$$T = \frac{I_t}{I_o} = \exp(-k_v.L) \quad (1)$$

where  $I_o$  and  $I_t$  are the strengths of the beams before and after passing through the medium respectively,  $k_v$  is the spectral absorbance coefficient ( $\text{cm}^{-1}$ ), and  $L$  is the beam path length (cm). The value of  $k_v$  for an individual spectral line can be defined as [10]:

$$k_v = S(T) \cdot \phi(\nu) \cdot N_d \quad (2)$$

where,  $S(T)$  is the line strength at a certain wavenumber  $\nu$  ( $\text{cm}^{-1}/\text{molecules} \cdot \text{cm}^{-2}$ ),  $\phi(\nu)$  is the line shape function ( $1/\text{cm}^{-1}$ ),  $N_d$  is the number of the absorbing molecules per unit volume, and can be calculated as

$$N_d = N_L \cdot P_T \cdot X_{abs} \cdot \left( \frac{296}{T} \right) \quad (3)$$

where  $T$  is the temperature (K),  $P_T$  is the total pressure (atm),  $X_{abs}$  is the mole fraction of absorbing medium, and  $N_L$  is the Loschmidts' number,  $N_L = 2.447 \times 10^{19}$  ( $\text{molecules}/\text{cm}^3/\text{atm}$  at 296 K).

### Experimental setup

Figure 1 presents a photograph of the experimental arrangement which was used to study the axisymmetric subsonic jet flow. A tunable diode laser (EP1392-DM-DX1) with salient characteristics similar to that described in [6] and [7], was modulated across the wavelength range between 1392 and 1393 nm by controlling the laser current with a frequency of 10 Hz. A jet nozzle with a nominal radius of 14 mm, was used to provide the apparatus with a flow of moist air. A plate with uniformly distributed 2 mm holes distributed around the nozzle was used to deliver a dry nitrogen co-flow for the jet of moist air. Nitrogen was also used to purge the water-vapour from the optical path, other than in the jet flow. The detected signal is received by an Auto-Balanced Photoreceiver model (Nirvana2017), which is connected into an oscilloscope and DAQ system (LabVIEW) to monitor and record the data. The test section has been designed to move in two axes, to allow the laser to traverse the jet at various radial and streamwise locations. The conditions are monitored by using a hygrometer ( $\pm 2\%$ ), thermocouple (K-type  $\pm 1^\circ\text{C}$ ), and Vernier mercury barometer ( $\pm 0.05$  kPa). A volumetric flow meter ( $\pm 0.001$  LPM) was also used to maintain the mixing ratio (mass of nitrogen/mass of air) constant at  $\text{MR} = 1.5$ .

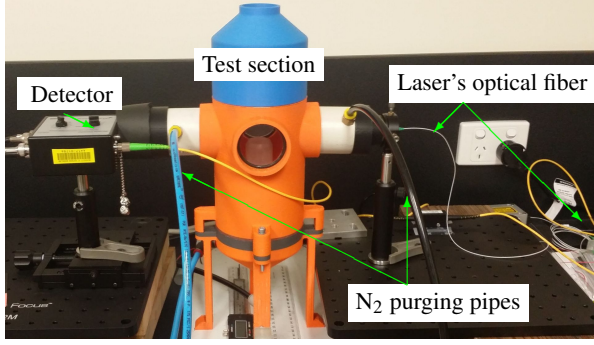


Figure 1: Photograph of the H<sub>2</sub>O jet apparatus.

### Measurement methodology

The experiment is arranged as shown in Figure 2. The diode laser was scanned across the selected spectral range, using a sawtooth current modulation profile to provide a range of wavenumber from 7179 to 7183 cm<sup>-1</sup>. The laser beam is split into two: the reference beam  $I_{Ref}$  was fed directly into the reference photodiode, and the signal beam  $I_{Sig}$  was transmitted through the jet. An attenuator is used to control the laser power in the reference beam  $I_{Ref}$ . The photoreceiver was used in the linear mode to balance the splitting ratio between the reference beam and the transmitted beam giving  $I_{Ref} \simeq 2I_{Sig}$ . Three output voltages from the differential detector were recorded: signal monitor, log output and linear output. The laser beam was arranged to pass through the jet at three distances downstream of the nozzle exit: 5, 10, and 15 mm. At each distance, TDLAS measurements of water-vapour absorbance were made at radial locations between stations 0 and 20 mm from the nozzle centre-line in increments of 1 mm.

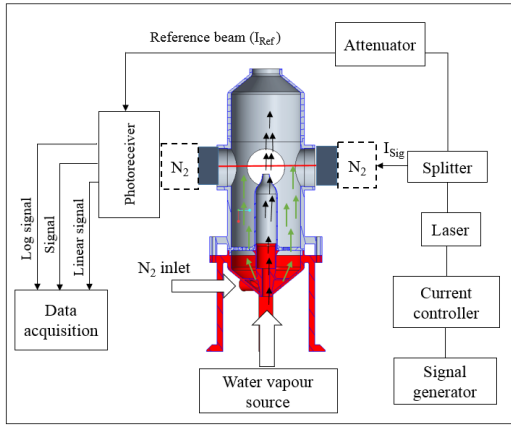


Figure 2: Schematic of the experiment setup.

### Balanced detection technique

The balanced detection or log-ratio method has been adopted to minimise the common-mode noise and more effectively amplify the absorption signals of interest. The power split ratio is the ratio of the reference beam power  $I_{Ref}$  to the transmitted beam power  $I_{Sig}$  [4], and the log voltage output signal is given by:

$$V_{log} = -G \log \left( \frac{I_{Ref}}{I_{Sig}} - 1 \right) \quad (4)$$

where  $G$  is gain of the detector. The photoreceiver has the best performance for noise rejection at  $I_{Ref} \simeq 2I_{Sig}$ .

### Signal post-processing

#### Voigt fitting

A mean signal was obtained from approximately 100 scans at each station. A Voigt fit was applied to smooth the data in a form suitable for comparison with the simulated theoretical profile. The Voigt fitting was based on the method which is well described in [1, 9]. A MATLAB script was used to define initial Voigt lineshape parameters for the fitting process, including: peaks maximum absorbance magnitude, peaks central wavenumber, Gaussian width, and Lorentzian width. Figure 3 shows an example of one of the acquired absorbance profiles and the associated Voigt fit.

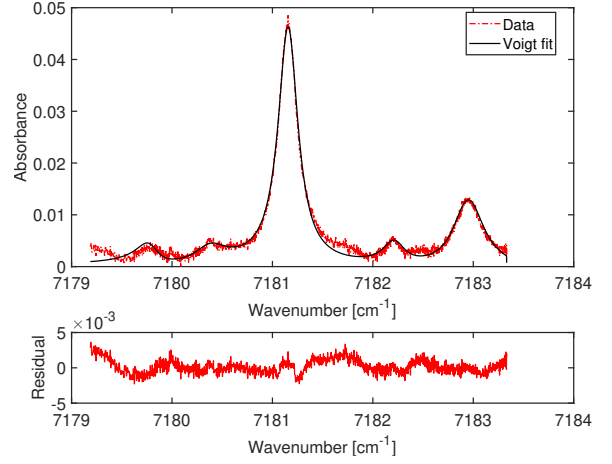


Figure 3: Voigt fit and residual for data obtained at 5 mm from nozzle exit,  $r = 3$  mm,  $P = 94$  kPa,  $T = 294$  K, and  $RH = 70\%$ .

#### Abel inversion algorithm

The objective of this study is to recover the radial distribution of the jet water-vapour concentration,  $F(r)$ . Figure 4, illustrates the nomenclature associated with the Abel inversion. The collected data represents a line-of-sight integrated effect and is called the projection data. The relationship between the projection data  $I(y)$  and the radial distribution  $F(r)$ , can be described with Abel's equation [2]:

$$I(y) = 2 \int_y^R \frac{F(r)}{\sqrt{r^2 - y^2}} dr \quad (5)$$

Different approaches have been developed in the literature [2] to reconstruct the  $F(r_i)$  distribution. In this study, the Three-Point-Deconvolution (TPD) method has been adopted, as it has a low noise relative to other methods [2]. The Abel inversion equation can be written as:

$$F(r) = -\frac{1}{\pi} \int_r^R \frac{I'(y)}{\sqrt{y^2 - r^2}} dy \quad (6)$$

#### Analysis method — synthetic and actual data

All Abel inversion algorithms have two main problems: the discontinuity of Equation 6 at  $y = r$ , and its reliance upon the first derivative of  $I(y)$ , which requires smooth data [2]. In practice, however, the experimental data will contain some noise. To test the Abel inversion and other aspects of the analysis method, synthetic data was generated according to the following steps:

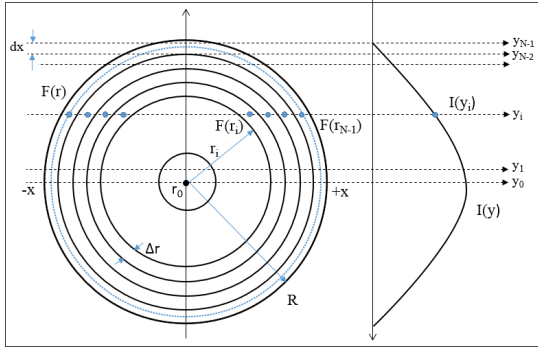


Figure 4: Field discretisation for Abel inversion.

1. Specify a concentration profiles for  $\text{H}_2\text{O}$  vapour,  $C(r)$  that is representative of the profiles encountered in the experiments. Specify constant temperature and pressure conditions that do not vary with radius.
2. Identify the coefficient of absorbance  $k_v$ , for a wavenumber range between  $7179$  and  $7183 \text{ cm}^{-1}$  as a function of radius for the conditions specified in Step 1 using the HITRAN database.
3. Determine the synthetic integrated absorbance for the chosen range of wavelengths by performing a line-of-sight integration (in the  $x$ -axis direction, effectively from  $(-20$  to  $+20)$ , at the same number of  $y$ -locations used in the experiments.
4. Add a representative level of noise to the synthetic transmission/absorption data. A signal-noise-ratio ( $SNR$ ) of  $20$  dB was chosen.

To analyse both the synthetic and actual data, the following steps were taken:

- At each value of  $y$ -location where data is available, Voigt fitting was used to smooth data, as shown in Figure 5 (for the case of synthetic data).
- Apply the inverse Abel transformation to the absorption data (which is a function of  $y$ ) to obtain the coefficient of absorbance  $k_v$  as a function of  $r$ .
- Identify concentration, pressure and temperature which minimise the error between the coefficient of absorbance  $k_v$  data and the results from the HITRAN database over a specified range of wavenumbers. This fitting is achieved by using the Levenberg-Marquardt optimization approach between the experimental absorbance coefficient  $k_v$  and the simulated theoretical spectra profile. The theoretical spectral profile was estimated using MATLAB script with aid of HITRAN database 2012 [8].

When working with the synthetic concentration data, it is then possible to define the error in the concentration as a function of radius. Figure 6 show the original synthetic concentration profile and the concentration profile that is deduced from the inverse Abel transformation and the HITRAN fitting method described above. The wavenumber range used for fitting the absorbance coefficient in the case of the synthetic data was from  $7179 \text{ cm}^{-1}$  to  $7183 \text{ cm}^{-1}$ , for each radial location.

In the case of the actual experimental data the wavenumber range used for fitting the absorbance coefficient varied depending on the position within the jet. Normally, the range from

$7179 \text{ cm}^{-1}$  to  $7183 \text{ cm}^{-1}$  was used, but when the concentration fell below  $0.004$ , the wavenumber range from  $7181.2 \text{ cm}^{-1}$  to  $7181.25 \text{ cm}^{-1}$  was used. Figure 7, shows an example of the deconvolved absorbance coefficient profile data and the fitted theoretical data.

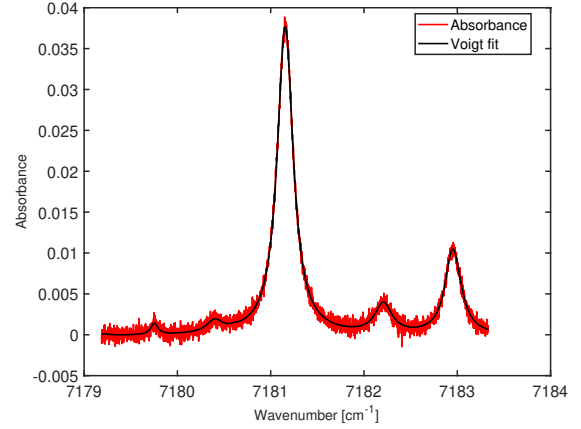


Figure 5: Integrated spectral absorbance at the centre of the specified (synthetic) concentration profile,  $SNR = 20$  dB,  $P = 94$  kPa, and  $T = 294$  K.

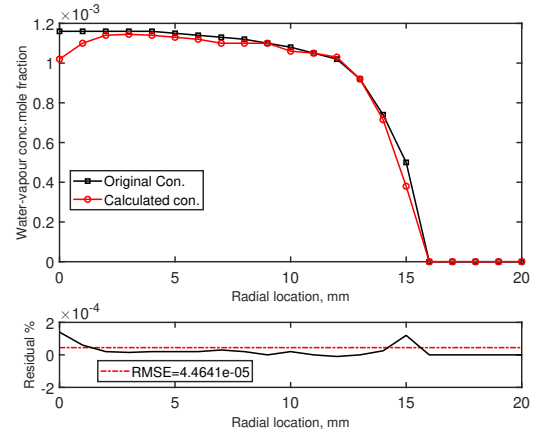


Figure 6: Comparison between the specified (synthetic) concentration profile and the profile obtained from Abel inversion method.

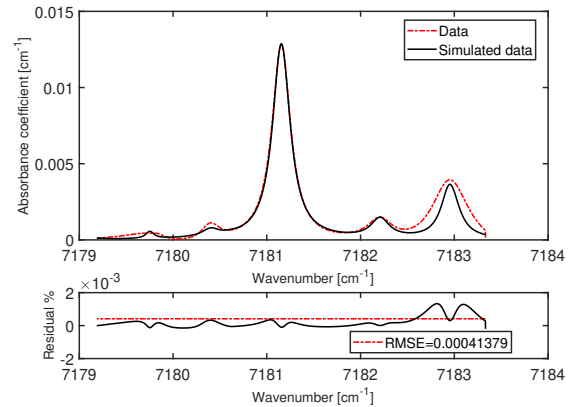


Figure 7: Reconstructed absorbance coefficient profile at  $10$  mm from nozzle exit,  $r = 4$  mm,  $P = 94$  kPa,  $T = 294$  K, and  $RH = 70\%$ .

## Results and Discussion

Figures 8 and 9 show the measured absorbance profiles (the projection data) at 5 mm and 15 mm downstream of the nozzle exit. Using the methods described in the previous section, the radial distribution of the water-vapour concentration within the jet was reconstructed at the three locations downstream of the nozzle exit: 5, 10, and 15 mm, as shown in Figure 10. The results indicate that the jet was narrowest and contained the highest concentration of water vapour at the station closest to the nozzle exit (5 mm). At the location 15 mm downstream of the nozzle exit, the centreline water vapour concentration was lower than at the 5 mm and 10 mm stations. Such features are consistent with those expected for a mixing jet. However, the jet flow established in this work deserves further investigation because the results at the 5 mm station indicate a peak in water vapour concentration at a radius of approximately 10 mm which is an unusual feature for a mixing jet.

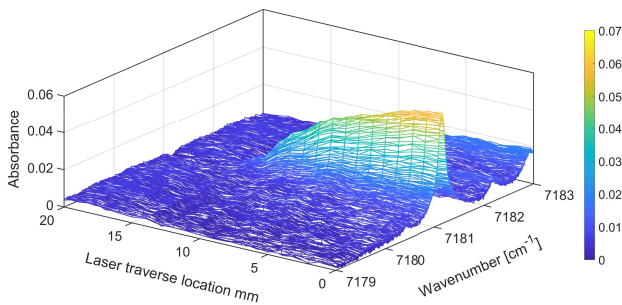


Figure 8: Absorbance results at 5 mm downstream of the nozzle exit.

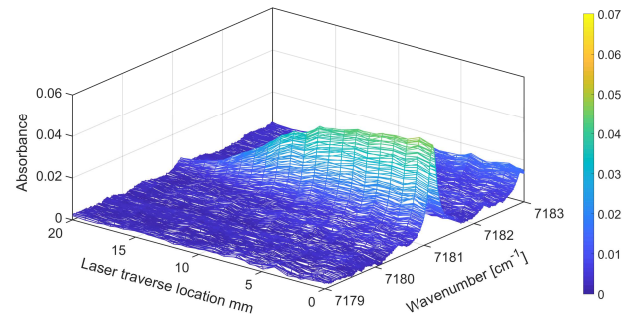


Figure 9: Absorbance results at 15 mm downstream of the nozzle exit.

## Conclusions

This paper has shown that it is possible to use the inverse Abel transformation to determine the water vapour concentration in an axisymmetric jet flow profile. An experimental TDLAS study was performed using the log-ratio detection technique. To determine the radial distributions of mole fraction within a moist air jet at different locations from the nozzle exit. Based on analysis using synthetic data, the current method should be capable of yielding concentration to within an accuracy of 5% for the conditions considered herein.

## Acknowledgments

The authors would like to thank the Higher Committee of Education Development (HCED) in Iraq for sponsoring A. Al-manea's Doctoral program. Dr. M. Zhao is also thanked for his assistance in the application of the Abel inversion technique.

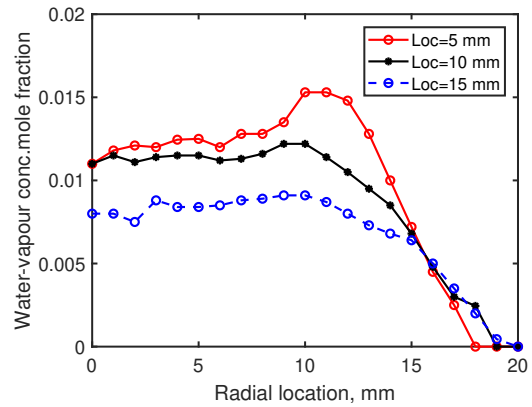


Figure 10: Reconstructed water-vapour concentration mole fraction.

## References

- [1] Abrarov, S. M., and Brendan M. Quine, Efficient algorithmic implementation of the Voigt/complex error function based on exponential series approximation, *Applied Mathematics and Computation*, **218**, 2011, 1894-1902.
- [2] Dasch, Cameron J., One-dimensional tomography: a comparison of Abel, onion-peeling, and filtered back projection methods, *Applied optics* **31**, 1992, 1146-1152.
- [3] Grazzini, et al., Ejectors for Efficient Refrigeration: Design, Applications and Computational Fluid Dynamics, *Springer*, 2018.
- [4] Griffiths AD, Houwing AF., Measurements of temperature and water vapour concentration in a scramjet combustor, *15<sup>th</sup> AFMC Conference*, 2004.
- [5] Guha, et al., Tomographic laser absorption spectroscopy using Tikhonov regularization, *Applied optics*, **53**, 2014, 8095-8103.
- [6] O'carroll, et al., Dynamic characteristics of InGaAs/InP multiple quantum well discrete mode laser diodes emitting at 2  $\mu$ m, *Electronics Letters*, **50**, 2014, 948-950.
- [7] Phelan, et al., In<sub>0.75</sub>Ga<sub>0.25</sub>As/InP Multiple Quantum-Well Discrete-Mode Laser Diode Emitting at 2 $\mu$ m, *IEEE Photonics Technology Letters*, **24**, 2012, 652-654.
- [8] Rothman, et al., The HITRAN2012 molecular spectroscopic database, *Journal of Quantitative Spectroscopy and Radiative Transfer*, **130**, 2013, 4-50.
- [9] Wells, R. J., Rapid approximation to the Voigt/Faddeeva function and its derivatives, *Journal of Quantitative Spectroscopy and Radiative Transfer*, **62**, 1999, 29-48.
- [10] Yun, et al., Calculation of infrared absorption coefficients of dissolved gases in transformer oil, *International Conference ICECE*, 2010, 3431-3434.
- [11] Zhou, Xin, Diode laser absorption sensors for combustion control, *Doctoral dissertation*, Stanford University, 2005.